# LAMINAR AIRFOIL DESIGN UNDER UNCERTAINTIES USING THE DLR $\gamma$ TRANSITION MODEL

J. Parekh*†, P. Bekemeyer*†, S. Helm*†, D. G. François†, C. Grabe*†

* Cluster of Excellence SE$^2$A – Sustainable and Energy-Efficient Aviation, TU Braunschweig, Deutschland
† Deutsches Zentrum für Luft- und Raumfahrt (DLR), Institut für Aerodynamik und Strömungstechnik, Braunschweig/Göttingen, Deutschland

Abstract

The development of energy-efficient aircraft is crucial for achieving sustainable, zero-emission air travel. Achieving sustainability in aviation necessitates strategies to reduce fuel consumption, including the implementation of low-drag wing designs and harnessing laminar flow. However, designing laminar aircraft requires intricate methodologies due to sensitivity to environmental and operational variations. This study addresses the challenge of designing energy-efficient aircraft by employing computational fluid dynamics models and advanced optimization under uncertainty techniques. We show the successful application of the surrogate-based optimization and uncertainty quantification approach in the optimization of airfoil drag enabling a natural laminar airfoil (NLF) design. The optimization process employs surrogate models trained using the data from high-fidelity airfoil simulations using - (i) a boundary layer code coupled with linear stability method, and (ii) a recently developed transition transport model. Accuracy of the surrogate models is improved using an active sampling strategy. The robust optimization approach accounts for uncertainties in environmental and operational conditions, providing a more comprehensive understanding of their impact on key design parameters. Contrary to conventional deterministic aerodynamic design optimization, our results demonstrate the effectiveness and accuracy of optimization under uncertainty for achieving robust NLF airfoil designs. The robust optimums favor a delayed transition location w.r.t. the instabilities, unlike their deterministic counterparts that feature sudden transitions triggering fully turbulent flow. This study advances the field by offering a practical and reliable methodology for developing energy-efficient airfoil. The application of these advanced optimization techniques and uncertainty quantification methods holds significant promise for the broader field of aerospace engineering, offering a pathway towards more robust designs.

Keywords
Robust Design Optimization, Surrogate Based Uncertainty Quantification,
Laminarization, Transition Modeling

NOMENCLATURE

| | |
|---|---|
| $\alpha$ | angle of attack |
| $c$ | chord length |
| $C_D$ | drag coefficient |
| $C_L$ | lift coefficient |
| $C_M$ | moment coefficient |
| $C_P$ | pressure coefficient |
| DC | drag count |
| $J$ | objective function |
| $M$ | Mach number |
| $N_{CF}$ | critical N factor for crossflow instabilities |
| $N_{TS}$ | critical N factor for Tollmien–Schlichting instabilities |
| PDF | probability density function |
| QoI | quantity of interest |
| $\boldsymbol{x}$ | design parameters |
| $x, z$ | x and z coordinates |
| $x_{Tr}$ | x-coordinate of transition location |
| $\xi$ | uncertainty parameters |

## 1. INTRODUCTION

In commercial aviation, an ongoing need exists to decrease fuel usage. This imperative arises from the necessity to fulfill strict environmental objectives established by aviation regulatory bodies. The European Commission delineates these ecological objectives, stipulating a 75% decrease in $CO_2$ and a 90% decrease in $NO_x$ emissions per passenger kilometer by



doi: 10.25967/610225

2050 [1]. Additionally, this endeavor aims to curtail operational expenses for airlines.

Over the course of aviation's evolution, the improvements in aircraft design have led to enhanced aircraft performance. Consequently, commercial aircraft have gradually become highly efficient. Nonetheless, given the fundamental design of aircraft i.e. tube and wing has predominantly stayed unaltered, each subsequent attempt at redesign yields only moderate benefits in terms of efficiency. Hence, achieving a substantial advancement in aircraft performance necessitates the exploration of new aerodynamic configurations and the utilization of intricate airflow phenomena.

The passive extension of laminar flow, known as Natural Laminar Flow (NLF), aims for extending the laminar boundary layer which in turn reduced viscous drag thereby improving aerodynamic efficiency [2]. Achieving NLF requires suppressing boundary-layer instabilities that trigger flow transition. The advantages of NLF have been studied primarily for the low swept wings operating at reduced Reynolds numbers where the boundary-layer instabilities are negligible [3]. Higher Reynolds numbers and sweep angles trigger crossflow instabilities near the leading edge leading to a fully turbulent flow [4]. However, pressure profiles that counteract crossflow instabilities can be achieved via shape design, even without any active flow-control devices such as suction of boundary layer [5]. This is accomplished in NLF airfoil design through careful adjustment of the pressure distribution [6, 7].

The approach to design laminar wings involves using inverse design methods based on linear stability theory [6, 8]. These methods aim to create wing designs that maintain laminar flow by specifying desired pressure distributions. The pressure distribution features - an initial acceleration at the leading edge to reduce crossflow (CF) instability and a favorable pressure gradients to dampen Tollmien–Schlichting (TS) instabilities. Shock waves are then needed to slow down the flow, and the rear shape is adjusted to meet lift requirements. In this process, experts define the target pressure distribution for a specific flight condition, and inverse design techniques shape the wing accordingly, often followed by manual iterations for fine-tuning. Despite these efforts, this approach might not lead to an optimal design. Direct optimization methods are emerging as an alternative, offering better exploration of the design space. Well-defined design optimization problems can generate configurations with pressure distributions similar to expert-defined ones and often yield better results compared to inverse design methods.

The field of aerodynamic shape optimization is fairly established in academia and industry [9]. For instance, direct shape optimization has been used in designing airfoils and wings to achieve natural laminar flow [10]. Previously, NLF airfoils have been designed across various Mach numbers and lift coefficients to obtain a robust configuration [11]. In that work, the optimization aimed at minimizing a linear combination of the mean and standard deviation of the drag coefficient. An effective implementation of NLF is complicated due to the sensitivity of the transition location to the surface, the flow quality, the environmental and the operational conditions [12]. To account for such instabilities triggering transition, a robust design optimization for laminar airfoil under critical $N$-factor uncertainty has been proposed [13]. In that work, a low-fidelity tool XFOIL in combination with a boundary-layer solver and $e^N$ transition model was used to compute the aerodynamic quantities of interest. More recently, an efficient bilevel approach for optimization under uncertainty has been proposed [14], where the authors considered the uncertainty not only in the $N$-factors but also in the operational conditions.

Real-world applications of robust design methodologies addressing the environmental and operational conditions related to NLF problems are notably lacking. Previous efforts largely focused on low-fidelity simulations incorporating only 2D instabilities, curtailing their suitability for swept-wing scenarios. Moreover, the environmental uncertainties have been studied for the $e^N$ method and a suitable analysis is lacking for the recently developed intermittency-based transition model. The DLR TAU code offers steady RANS simulations coupled with a boundary layer code and linear stability method ($e^N$), on the one hand and a recently developed intermittency-based transition transport model (DLR $\gamma$) on the other hand. In the present study, we primarily focus on - (i) establishing a probabilistic framework for effectively designing robust NLF transonic airfoil resilient against the uncertain environmental and operational conditions at high sweep and Reynolds number, and (ii) comparing the robust (and deterministic) optimums obtained using the two transition modeling approaches, namely $e^N$ method and DLR $\gamma$ model.

The sections in this paper are structured as follows. Section 2 introduces the bilevel robust optimization framework that employs surrogate models for optimization and uncertainty quantification. Section 3 presents the setup of transonic airfoil (RAE2822) optimization under uncertainty including the formulation of the optimization problem with constraints, flight conditions, transition models and the associated environmental uncertainties, parameterization of design space and the numerical model used to compute the aerodynamic QoIs. The results obtained from the deterministic and robust optimization using both the transition models are presented in 4. Finally, conclusions are presented in section 5.

## 2. ROBUST OPTIMIZATION FRAMEWORK

Solving a global optimization problem may require a large number of function (black-box) evaluations depending on the design space and the non-linearity of the function. This can rapidly turn intractable and infeasible, e.g. when - (i) the design space is high-dimensional, and/or (ii) the function evaluation is expensive (e.g. a typical CFD simulation). Moreover,

due to the evaluation of statistics at each iteration (discussed in subsequent section), the computational cost of the optimization under uncertainties further increases by several orders. Discussed next is an efficient surrogate-based robust optimization framework that has been proven to overcome such high computational cost [15].

### 2.1. Problem Definition

Let $Y \in \mathbb{R}$ be the quantity of interest (QoI) which is usually a performance measure such as drag coefficient, depending (mostly non-linearly) on the design variables $\boldsymbol{x} \in \mathbb{R}^d$ at operating conditions $\boldsymbol{A}$. The goal of deterministic optimization is to find an optimal set of design variables $\boldsymbol{x}^*$ at constant (nominal) operating conditions $\boldsymbol{A}_0$ while satisfying $k$ constraints on the design variables,

$$\begin{aligned} \boldsymbol{x}^* &= \arg\min_x \{Y(\boldsymbol{x}, \boldsymbol{A}_0)\}, \\ g_i(\boldsymbol{x}) &\leq 0, \quad i = 1, 2, ..., k. \end{aligned} \tag{1}$$

Whereas, the robust optimization aims at finding an optimal design while considering the uncertainties $\boldsymbol{\xi} \in \mathbb{R}^m$ in environmental and/or operational conditions. Consequently, the QoI becomes a random variable, which in turn changes the problem from the optimization of the QoI towards the optimization of relevant statistic of the QoI. The statistic (e.g. mean, standard deviation, quantile etc.) of the QoI is computed using uncertainty propagation and is thereafter minimized by the optimizer. In this study, we consider the mean value of the QoI $\mu_Y$ and define the robust optimization problem as follows,

$$\begin{aligned} \boldsymbol{x}^* &= \arg\min_x \{\mu_Y(\boldsymbol{x}, \boldsymbol{\xi})\}, \\ g_i(\boldsymbol{x}) &\leq 0, \quad i = 1, 2, ..., k. \end{aligned} \tag{2}$$

### 2.2. Bilevel Surrogate-Based Approach for Optimization Under Uncertainty

A general-purpose framework of a bilevel surrogate model has been previously used for various robust design optimization problems consisting of moderate number of dimensions and uncertainties [14, 15]. As shown in Fig 1, the framework consists of two nested-loops combining a Surrogate-Based Optimization (SBO) strategy (outer loop), with a Surrogate-Based Uncertainty Quantification (SBUQ) method (inner loop). Each iteration in the optimization requires only the design variables $\boldsymbol{x}$ as the input to the SBO surrogate (red response surface) and has the statistic of the QoI as the output. Whereas the SBUQ surrogate (blue response surface), for given design variables, has the uncertainties $\boldsymbol{\xi}$ as the input and the QoI as the output (computed using the black-box function). The gradient-free robust optimization framework is particularly useful as the CFD simulations involving transition predictions using the $e^N$ method or the DLR $\gamma$ model that do not readily provide adjoint solutions. The overall efficiency of the framework is further enhanced by refining the vicinity of optimal solution using infill (adaptive sampling) strategies. Parallel evaluation of the design of experiment (DoE) and the in-built parallelization of the black-box CFD solver further adds to the efficiency of the framework.

#### 2.2.1. Optimization

The main objective of the bilevel framework's outer loop (SBO) is to perform an efficient optimization by using a low number of expensive black-box evaluations [16]. For this purpose a surrogate model is constructed which not only maps the design variables to the QoI but is also cheap to evaluate.
We use the SBO module of Surrogate-Modelling for AeRo-data Toolbox in pYthon (SMARTy) developed by DLR, German Aerospace Center [17]. This optimization module - (i) generates the initial DoE sampling in the design space and evaluates the objective function (and constraints), (ii) constructs a surrogate model for the objective function (and constraints), (iii) uses an active infill criteria to sequentially reach the optimum while evaluating the black-box solver for each proposed optimal design, and (iv) reconstructs the surrogate model(s) after every infill iteration. In this work, we use Sobol sequences for the DoE stage [18] and Kriging (Gaussian process regression) models as surrogates [19]. The infill criteria employed here is expected improvement (EI) method which is based on the normal distribution prediction (mean $\hat{y}(\boldsymbol{x})$ and standard deviation $\hat{\sigma}(\boldsymbol{x})$) of the objective function obtained from the Kriging surrogate at any given location $\boldsymbol{x}$ in design space [20]. Using the probability of improvement with respect to the current best sampled solution $y_{min}$, EI is defined defined as:

$$\begin{aligned} E[I(\boldsymbol{x})] = (y_{min} - \hat{y}(\boldsymbol{x}))\, \Phi\left(\frac{y_{min} - \hat{y}(\boldsymbol{x})}{\hat{\sigma}(\boldsymbol{x})}\right) + \\ \hat{\sigma}(\boldsymbol{x})\phi\left(\frac{y_{min} - \hat{y}(\boldsymbol{x})}{\hat{\sigma}(\boldsymbol{x})}\right), \end{aligned} \tag{3}$$

where $\Phi$ and $\phi$ are the cumulative and probability distribution functions of the standard normal distribution, respectively. The EI infill method balances exploration with exploitation in the sense that a large expected improvement is present in the regions where a solution smaller than the current best is possible and/or in the regions where the model error is large.
The refining continues until the convergence criteria (L2 distance between consecutive design vectors or the EI values) or the maximum number of infill points (budget) is reached.

#### 2.2.2. Uncertainty Quantification

The aim of the bilevel framework's inner loop (SBUQ) is to efficiently propagate the input uncertainties towards the QoI, followed by accurately approximating the statistic of the QoIs to be used by SBO. To avoid the expensive classical Monte Carlo approach for un-

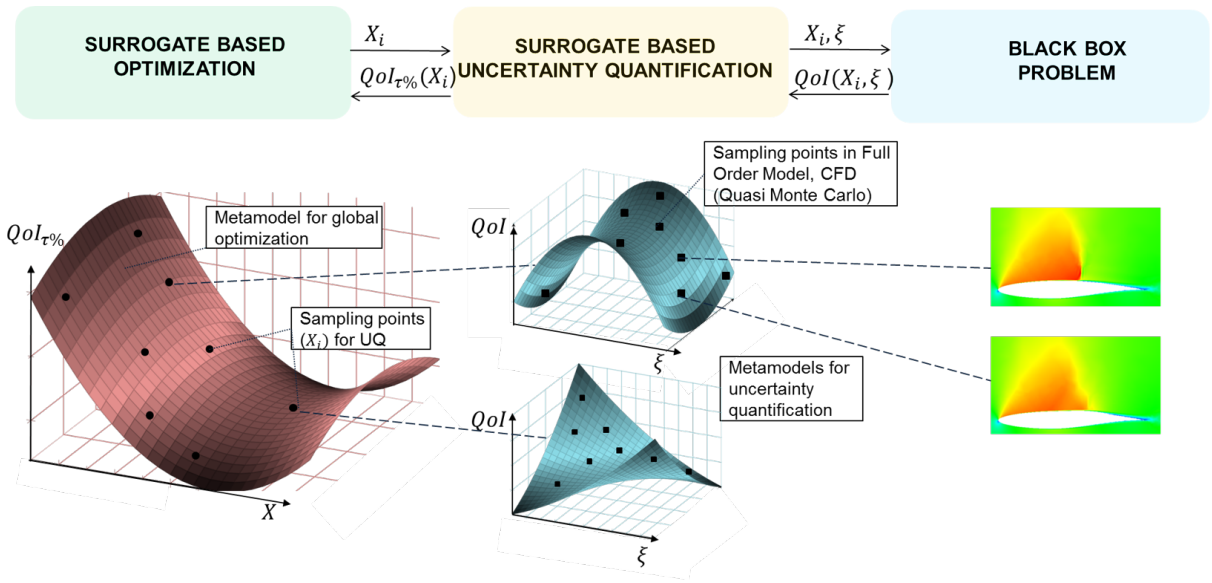


FIG 1. Bilevel approach for uncertainty quantification [15]: surrogate of statistics (left), surrogate of random variable (middle), and full-order model evaluation (right).

certainty quantification, we employ a surrogate-based approach to estimate the statistic. Based on the initial DoE generated using the stochastic space and its evaluations (black-box solves), a Kriging surrogate model is constructed that maps the uncertainties to the QoI. In order to increase the accuracy of the surrogate, a statistic based active infill criteria is used. In this study we use the infill criteria targeting the mean of QoI which requires a high global accuracy of the surrogate. To ensure an even sampling in the stochastic space, the infill criteria makes use of the prediction mean square error $\hat{s}(\boldsymbol{\xi})$ at any point $\boldsymbol{\xi}$ available in the Kriging surrogate. A new sample is sequentially added (after updating the surrogate) in the location $\boldsymbol{\xi}^*$ where the product of the joint probability distribution function of the input uncertainties $\mathrm{PDF}_\xi$ and the error estimate is maximum. The resulting minimization problem is defined as:

$$\boldsymbol{\xi}^* = \arg\min_{\boldsymbol{\xi}} \{ -\mathrm{PDF}_\xi(\boldsymbol{\xi})\, \hat{s}(\boldsymbol{\xi}) \} \tag{4}$$

The $\mathrm{PDF}_\xi$ term favors the sampling of location with high probability in the stochastic space while the error term $\hat{s}(\boldsymbol{\xi})$ favors the sampling from regions of low surrogate accuracy. Differential evolution is used to find the optimum location in the surrogate. The statistic of QoI is obtained using a large number of Quasi Monte Carlo samples evaluating the surrogate model.

## 3. ROBUST DESIGN OF A TRANSONIC AIRFOIL: SETUP

In this section we present the formulation of the deterministic and robust transonic airfoil optimization, characterization of the design space and the uncertainties as well as the numerical model used as the black-box solver.

### 3.1. Flight Conditions for Robust Optimization

The deterministic and the robust optimization are used to determine an optimal transonic airfoil design operating under the design conditions of: Mach number 0.78, coefficient of lift 0.7, Reynolds number $23 \times 10^6$ and sweep angle of $27^o$. Based on the Fokker 100 and Advanced Technologies Testing Aircraft System (ATTAS) flight tests [21, 22], due to the attachment line and crossflow instabilities, a premature transition to turbulence is inevitable at higher Reynolds number and sweep angles. Attachment line transition can be mitigated by constructive features such as anti-contamination devices or Gaster bumps and is, therefore, excluded from the present investigation. In contrast to that, crossflow instabilities can be suppressed by adequate profiling of the wing, at the cost of increasing Tollmien-Schlichting instability. This trade-off can be efficiently handled using numerical optimization, enabling the extension of laminarity even at higher Reynolds number and sweep angles.

### 3.2. Deterministic and Robust Optimization

In the present study, the deterministic optimization solves for the optimum design $\boldsymbol{x}^*$ that minimizes the drag coefficient at a constant (nominal) value of Mach number and lift coefficient. The maximum airfoil thickness normalized by chord length $t/c_{max}$ is set to be greater than $t/c_{max,0} = 0.11$:

$$\begin{aligned} \boldsymbol{x}^* &= \arg\min_{x} \{C_D(\boldsymbol{x}, M, C_L)\} \\ \text{s.t.} \quad & t/c_{max} \geq t/c_{max,0} \end{aligned} \tag{5}$$

The constant lift coefficient is handled by the CFD solver by iteratively adjusting the angle of attack. The maximum thickness constraint is set as a constraint

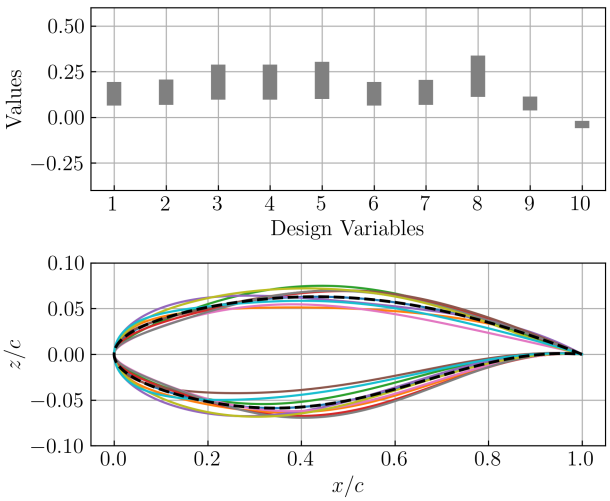


FIG 2. CST design variable bounds used for optimization (top). RAE2822 airfoil (dashed) and sample airfoil profiles (colored) in the design space (bottom).

in the optimization process.

In order to approximate realistic flight conditions, the robust optimization incorporates both environmental and operational uncertainties $\boldsymbol{\xi}$. As discussed earlier, the QoI ($C_D$) becomes a random variable, the statistic of which is therefore optimized. In order to obtain an overall good performance, in this study, the minimization of the mean values of the drag coefficient $\mu_{C_D}$ is sought.

$$\begin{aligned} \boldsymbol{x}^* &= \arg\min_x \{\mu_{C_D}(\boldsymbol{x}, \boldsymbol{\xi})\} \\ \text{s.t.} \quad & t/c_{max} \geq t/c_{max,0} \end{aligned} \tag{6}$$

### 3.3. Parameterization of Design Space

The objective function in both deterministic and robust optimization depends on the design variables $\boldsymbol{x}$ that describe the shape of the airfoil. In this study, we use the class shape function transformations (CSTs) to describe and change the profile of an airfoil over the optimization iterations [23]. The parameterization represents a two-dimensional geometry by the product of a class function $C(x/c)$, and a shape function $S(x/c)$ based on Bernstein binomials, plus a term that characterizes the trailing edge thickness:

$$\begin{aligned} \frac{\mathrm{z}}{\mathrm{c}} &= C\left(\frac{\mathrm{x}}{\mathrm{c}}\right) S\left(\frac{\mathrm{x}}{\mathrm{c}}\right) + \frac{\mathrm{x}}{\mathrm{c}} \frac{\Delta z_{TE}}{c} \\ C\left(\frac{\mathrm{x}}{\mathrm{c}}\right) &= \left(\frac{\mathrm{x}}{\mathrm{c}}\right)^{N_1} C\left(1 - \frac{\mathrm{x}}{\mathrm{c}}\right)^{N_2} \quad \text{for} \quad 0 \leq \frac{\mathrm{x}}{\mathrm{c}} \leq 1 \\ S\left(\frac{\mathrm{x}}{\mathrm{c}}\right) &= \sum_{i=0}^{n} \left[ X_i K_{i,n} \left(\frac{\mathrm{x}}{\mathrm{c}}\right)^i \left(1 - \frac{\mathrm{x}}{\mathrm{c}}\right)^{n-i} \right] \end{aligned} \tag{7}$$

where $K_{i,n} = \frac{n!}{i!(n-i)!}$. The exponents $N_1$ and $N_2$ define the type of geometry to be represented. An airfoil, e.g. is represented by $N_1 = 1/2$ and $N_2 = 1$, adhering to the fact that the term $\sqrt{x/c}$ yields round leading edges, whereas $(1 - x/c)$ results in sharp trailing edges. The weight factors $X_i$ is representing the design variables. The CST parameterization guarantees C2 continuity of the surfaces and captures the space of smooth airfoil shapes. Ten design parameters are used to define this parameterization (five for the upper surface and five for the lower surface). The theoretical bounds of the CST parameters is $[-1, 1]$. However, in order to avoid unrealistic designs, we restrict the design space with respect to the baseline transonic airfoil (RAE2822) shape such that the CST bounds are $\boldsymbol{x}_0(1 \pm 0.3)$, i.e. $\pm 30\%$ of baseline design $\boldsymbol{x}_0$. This not only avoids nonphysical shapes but also facilitates the convergence of the optimizer. Fig 2 shows the bounds of the design variables and a few sample airfoil profiles around the baseline.

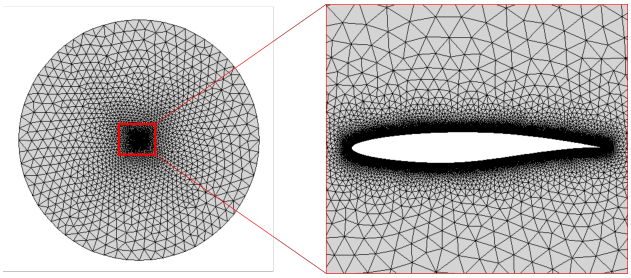

FIG 3. CFD grid of the baseline (RAE2822) airfoil used in the optimization problem. Every iteration in the optimization performs a mesh deformation.

### 3.4. Numerical Model

The flow around the airfoil is modeled using the DLR, German Aerospace Center, CFD solver TAU [24]. The aerodynamic quantities of interest are obtained by solving the Reynolds-averaged Navier-Stokes (RANS) equations in combination with the $k - \omega$ SST turbulence model. The solver settings include - a 4w multigrid cycle, a backward Euler solver for pseudo time integration, a central flux discretization scheme and an infinite swept-wing formulation to account for cross flow effects (2.5D analysis) [25]. The unstructured mesh with 150,000 cells and 1024 surface nodes is shown in Fig 3.

To predict the transition location we employ two different methods, namely the most commonly used $e^N$ method [26] and the recently developed DLR $\gamma-$CAS model [27]. The purpose of using two models is to make a comparison study of the optimums obtained and assess their robustness towards the environmental and operational uncertainties.

The $e^N$ method is validated through wind-tunnel and flight tests [8] and, therefore, commonly used for transition prediction in the industry. The TAU transition module [28] offers multiple tools for streamline-based transition prediction, e.g. including the $e^N$ method. In the present work the boundary-layer data is determined by the compressible conical boundary-layer code COCO [29]. Based on this data, the boundary-layer stability is analyzed by the linear-stability-theory (LST) based code LILO [30]. The

resulting $N$-factors are evaluated by the two-N-factor method. This means that transition is determined where the empirically determined critical N-factor envelope for Tollmien-Schlichting transition ($N_{TS}$) and crossflow transition ($N_{CF}$) is exceeded.
The DLR $\gamma$ model [27] consists of a transport equation for the intermittency $\gamma$, an auxiliary field variable taking values between 0 (laminar) and 1 (turbulent) and acting as a switch for the turbulence model. The model is derived from the $\gamma$-$Re_{\Theta_t}$ model [31] and includes advancements for the application of transport aircraft, e.g. the improved accounting of pressure gradient and compressibility on transition. This is achieved by means of a simplified version of the AHD transition criterion. In addition, the model offers an extension for crossflow transition [32] by means of the helicity and the C1 criteria. The model is successfully applied to laminar wings at high Reynolds numbers ($\sim 10^7$) and continuously validated [33]. However, for the configuration and operational conditions considered in the present study, we do not use the crossflow extension as it has been previously shown that the crossflow instabilities do not have a significant effect on the transition location [14].

### 3.5. Characterization of Uncertainties

In order to obtain laminar configurations that are robust against discrepancies in environmental and operational conditions, we must characterize and incorporate them in the optimization process.
The critical $N$-factors $N_{TS}, N_{CF}$ appearing in the $e^N$ method can be considered as an integral measure of the flow quality [8, 34]. These factors are highly dependent on freestream conditions such as the presence of clouds and the disturbance level (turbulent intensity) [35]. Moreover, the quality of the surface (imperfections) and acoustic disturbances can trigger the instability waves resulting in a decrease in critical $N$-factors (implying an early transition to turbulence). Therefore, the physical (environmental) uncertainties related to the $e^N$ method can be represented in terms of uncertainties in these critical $N$-factors. In a recent study [14], different possible distributions of uncertainties in critical $N$-factors were studied for a robust optimization of a NLF wing. Similarly, in this study, we characterize the uncertainties in the $N$-factors as two random variables with uniform distributions: $N_{TS} \sim \mathcal{U}[5, 14], N_{CF} \sim \mathcal{U}[4, 11]$. Such characterization of uncertain $N$-factors was considered to be a realistic approach accounting for instabilities due to clouds, imperfections and freestream turbulence [14].
Similarly, the environmental uncertainties related to the DLR $\gamma$ model can be represented in terms of random freestream turbulent intensity $T_u$. To approximate the distribution of the turbulent intensity, we use a direct relation between $N_{TS}$ and $T_u$ [36]:

$$N_{TS} = -8.43 - 2.4\, ln(T_u) \tag{8}$$

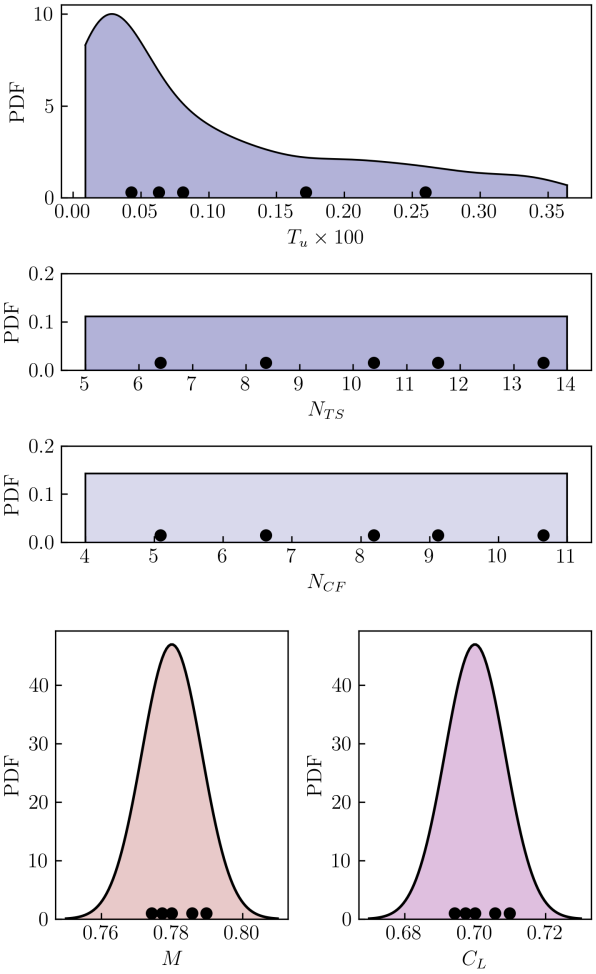


FIG 4. Distribution of environmental and operational uncertainties. For the $e^N$ method the $N$-factors ($N_{TS}, N_{CF}$) are considered to be uncertain and turbulent intensity $T_u$ is considered uncertain for the DLR $\gamma$ model. The dots represent a sampling example based on the distribution.

We construct a sampling-based distribution for $T_u$ using 1000 samples of $N_{TS}$ from the above-mentioned uniform distribution. The distributions for the $N$-factors and the freestream turbulent intensity are show in Fig 4 (left).
The operational values of Mach number and lift coefficient have been usually considered to be fixed. However, in a short-haul configuration the variability in the operational conditions during the cruise conditions can significantly affect the performance of the aircraft [37]. In this study, we consider Mach number and lift coefficient to be uncertain and model them using thin symmetric beta distributions centered around their nominal values as shown in Fig 4 (right).

## 4. ROBUST DESIGN OF A TRANSONIC AIRFOIL: RESULTS

In the following subsections we present the results for deterministic and robust optimization using both the transition models discussed in the previous section.

### 4.1. Deterministic Optimization at Nominal Values

The surrogate-based optimization (section 2.2.1) is used to solve the deterministic optimization problem defined in (5). The operational conditions Mach number and lift coefficient are set to their nominal values of 0.78 and 0.7, respectively. The optimization also assumes a constant value of $N$-factors (in $e^N$ method) and turbulent intensity (for DLR $\gamma$ model) which are set to $N_{TS} = 11.5, N_{CF} = 8.5$ and $T_u = 0.000247$. The value of turbulent intensity is based on $N_{TS}$ as per the relation in (8). The optimization budget, i.e. the number of DoE samples and the infill iterations are fixed to 100 and 20, respectively. This implies a DoE of ten samples with two infill points for each dimension of the design space $\mathbb{R}^{10}$, which is deemed to be reasonable for an accurate meta model construction [14, 15]. Fig 5 shows the optimization history for both the transition models. The DoE stage (1-100 iterations) consist of designs that are close to the baseline and have converged CFD solutions, resulting in a smooth and accurate surrogate model. The infill stage (101-120) as a result only takes a few iterations to reach the optimum. Designs that violate the constraint of maximum thickness are not considered as the (local) optimum by the optimizer.
In Fig 6, the optimum design and pressure profile are compared with those obtained using baseline (RAE2822). The optimal configuration for both the transition models is able to outperform the baseline by delaying the transition (almost) up to the shock. The optimized profile transition location for $e^N$ method and DLR $\gamma$ model is around 45 and 42%, respectively, resulting in a large extent of laminar flow as compared to the baseline configuration. This further leads to a reduction in drag by 22 and 19% for $e^N$ method and DLR $\gamma$ model, respectively. Despite of a high-dimensional design space, it is worth noting that the surrogate-based optimization is able to find

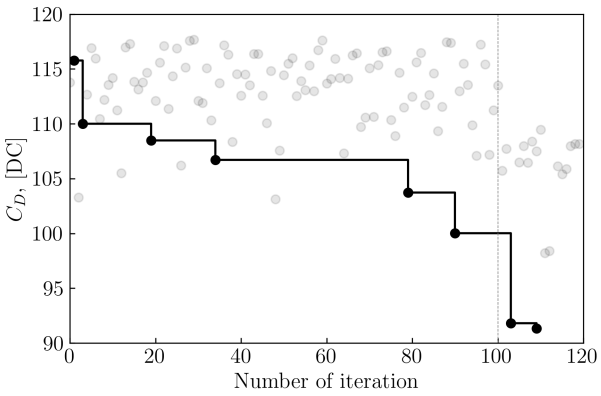


(a) $e^N$ method

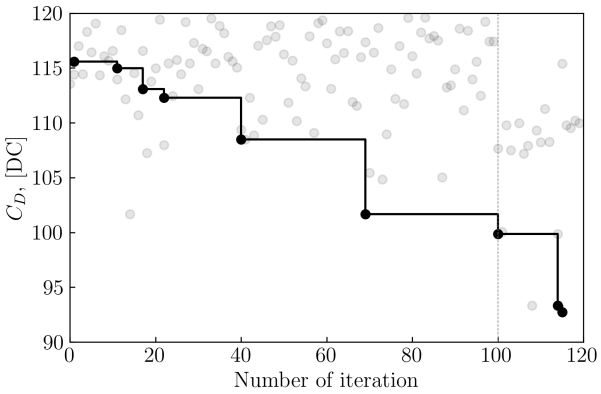


(b) DLR $\gamma$ model

FIG 5. Convergence history of deterministic optimization with 100 DoE and 20 Infill iterations. The gray dots represent each iteration while the step-wise connected black dots represent the run-time optimal designs. The iterations under the solid line are not considered optimal as they violate the constraint.

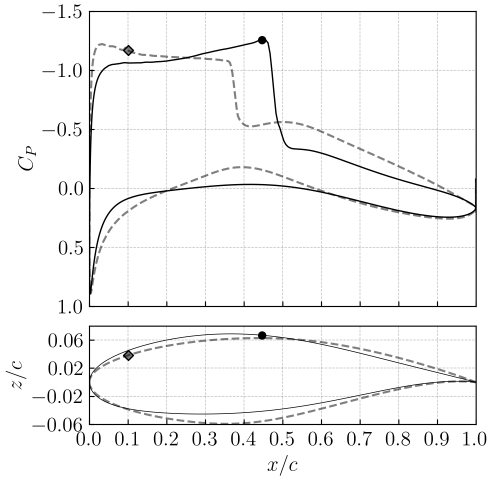


(a) $e^N$ method

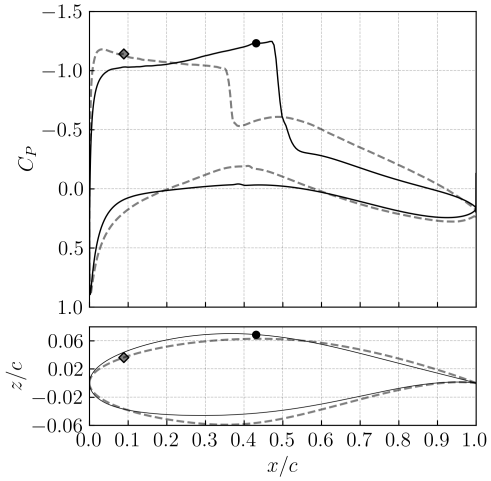


(b) DLR $\gamma$ model

FIG 6. Surface pressure distribution for the deterministic optimum. The dashed and the solid line represent the baseline (RAE2822) and the optimal airfoil, respectively. The corresponding dots denote the transition location ($x_{Tr}/c$).

a realistic laminar profile by merely enabling accurate transition prediction and drag minimization under a simple constraint. Also, worth mentioning is that there is only a subtle difference between the baseline as well as the optimum profiles of $e^N$ method and DLR $\gamma$ model. This is expected as the DLR $\gamma$ model relies on the "Simple-AHD" criterion [38] calibrated based on the LST-analysis database of the original AHD criterion [27]. It is believed that the main source of the (notably small) differences come from the fact that incompressible LST is used in combination with the $e^N$ method, whereas the "Simple-AHD" criterion is accounting for compressibility.

### 4.2. Performance of Deterministic Optimum under Environmental Uncertainties

Under the situations of varying environmental conditions, the performance of the deterministic optimum may deteriorate substantially. As discussed in [14], under the presence of uncertainties, the transition location of the deterministic optimum configuration may shift significantly upstream resulting in a fully turbulent flow. We employ a surrogate-based uncertainty quantification approach (section 2.2.2) to investigate the effect of environmental uncertainties on the aerodynamic performance of the deterministic optimum. A Kriging surrogate model is constructed using five DoE samples and one infill sample for each input random variable. Note that the infill criteria aims at improving the surrogate model based on the local error estimate (as discussed in section 2.2.2). The mean of the drag coefficient is computed using on 10,000 Quasi Monte-Carlo samples in the stochastic space evaluated with the surrogate and compared to a reference solution based on 200 Monte-Carlo samples evaluated directly using the black-box (CFD solver). As shown in Fig 7 the relative error in the mean and standard deviation of the drag coefficient for both the transition models was found to be less than 1 and 2.4%, respectively.
Fig 8 (a) and (d) shows ten random realizations of the pressure and transition locations obtained using the deterministic optimum design with uncertainty in $N$-factors (for $e^N$ method) and $T_u$ (for DLR $\gamma$ model), respectively. The details of the distribution of these uncertainties can be found in section 3.5. As observed for both the transition prediction approaches, the laminar to turbulent transition location has high variance and lies between 10 and 45%. i.e. from close to leading edge up to the shock. Also, the shock wave is found to be much stronger as compared to the baseline, further worsening the performance especially when the flow is already turbulent due to early transition. The deterministic optimum, therefore, operates in a fully turbulent mode for a considerable range of environmental parameters, implying a low resilience towards the uncertainties.

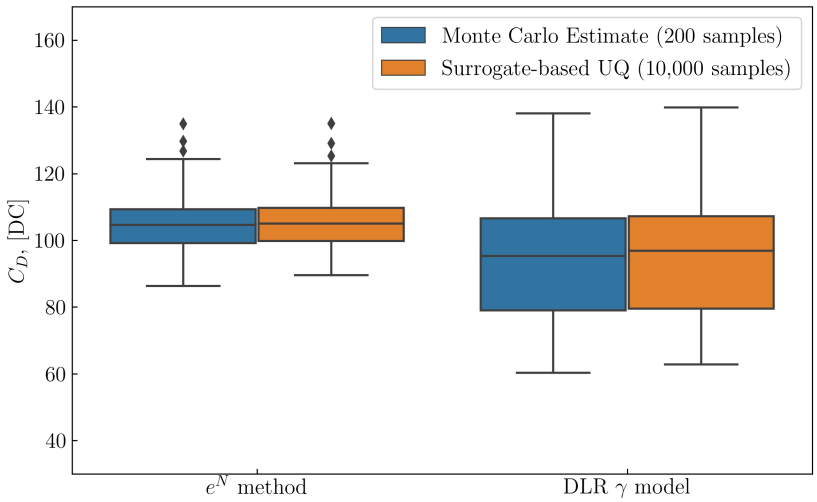


FIG 7. Comparison of statistics at deterministic optimal configurations under environmental uncertainties.

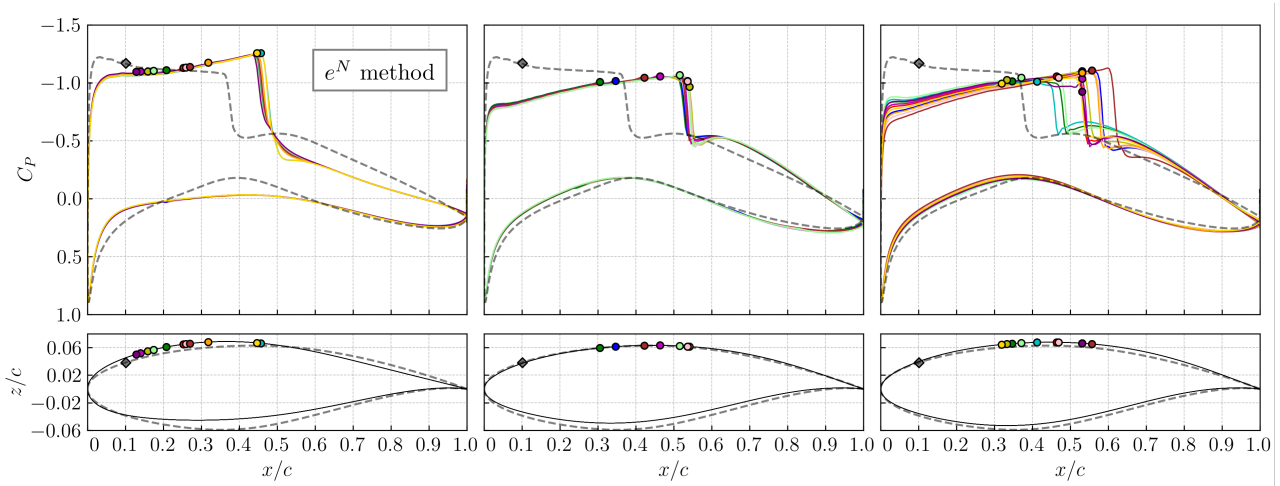


(a) Deterministic Optimum $(N_{TS}, N_{CF})$, $C_D$ (b) Robust Optimum $(N_{TS}, N_{CF})$, $\mu_{C_D}$ (c) Robust Optimum $(N_{TS}, N_{CF}, M, C_L)$, $\mu_{C_D}$

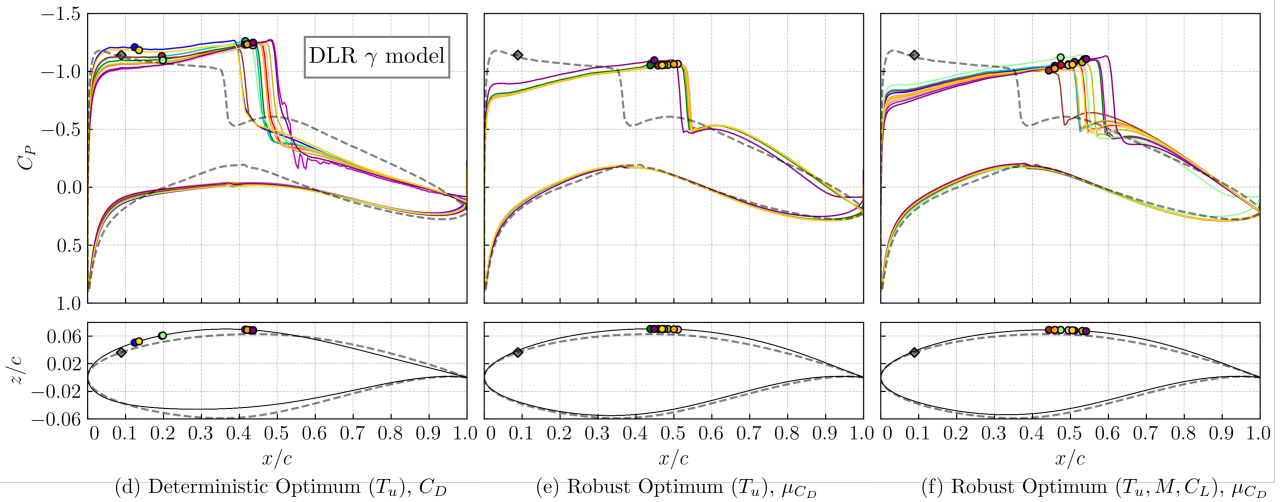


(d) Deterministic Optimum $(T_u)$, $C_D$ (e) Robust Optimum $(T_u)$, $\mu_{C_D}$ (f) Robust Optimum $(T_u, M, C_L)$, $\mu_{C_D}$

FIG 8. Random realizations of surface pressure coefficient (solid colored lines) and transition location (solid colored circles). The baseline design (RAE2822) is represented in dashed lines with its transition location in gray diamonds. Subfigures (a, b, c) and (d, e, f) correspond to $e^N$ method and DLR $\gamma$ model, respectively.

### 4.3. Robust Optimization under Environmental Uncertainties

As discussed earlier, the deterministic optimization results in an unstable configuration where a small variation in the environmental uncertainties can adversely affect the performance. Therefore, we seek a design based on robust optimization, i.e. optimization under uncertainties (section 3.2). We use the bilevel surrogate-based optimization to minimize the mean of drag coefficient under the presence of environmental uncertainties in the respective transition models. The surrogate-based uncertainty quantification was used in the inner loop to estimation the mean of drag coefficient (five DoE samples and one infill sample for each input random variable). Similar to deterministic optimization, a 100 DoE samples with 20 infill iterations were used for optimization. Fig 8 (b) and (e) shows ten random samples of the pressure and transition locations obtained using the robust optimum design for $e^N$ method and DLR $\gamma$ model, respectively. Unlike the deterministic optimum, the transition location for the robust optimum has significantly low variance and lies in a range from 30 to 55% and 43 to 52% for $e^N$ method and DLR $\gamma$ model, respectively. The range of transition location approximated using the Quasi Monte Carlo sampling in the surrogate were found to be close to that obtained from the random samples. A smooth variation in transition location and a weaker shock wave as compared to the baseline and deterministic optimum was observed. The robust optimum, therefore allows for delayed transition favouring an extended laminar region even at adverse environmental conditions, indicating resilience towards uncertainties.

### 4.4. Robust Optimization under Environmental and Operational Uncertainties

As discussed in section 3.5, in addition to the environmental conditions, the variability in the operational conditions may also contribute significantly to the variance in the aerodynamic QoIs. Therefore, we perform a robust optimization considering uncertainty not only in the $N$-factors (or turbulent intensity) but also in the Mach number and the lift coefficient. The number of DoE and infill samples (iterations) per input random variable (design variable) for uncertainty quantification (optimization) are kept the same. Fig 8 (c) and (f) shows realizations of the pressure and transition locations obtained using the robust optimum design for $e^N$ method and DLR $\gamma$ model, respectively. As observed, the smooth variation in the transition location is only slightly larger as compared to the robust optimum with only environmental uncertainties, with a range from 30 to 58% and 42 to 56% for $e^N$ method and DLR $\gamma$ model, respectively. However, the variance in the shock location as well as its strength increased significantly due to the addition of operational uncertainties. Overall, the optimum design still favors laminarity and is fairly robust against a relative larger input uncertainty.

### 4.5. Overall Performance of Optimums

Fig 9 shows the polar graphs of four aerodynamic QoIs - angle of attack $\alpha$, moment coefficient $C_M$, drag coefficient $C_D$ and transition location w.r.t. chord length $x_{Tr}/c$, at different optimums for $e^N$ method and DLR $\gamma$ model. The polygons (colored) represent the realizations of the normalized QoIs. The variation in polygon vertices can be considered to be inversely proportional to the robustness of the design. As observed, the deterministic optima (a, d) have high variances in all QoIs (except the moment coefficient) and thus can be deemed not robust towards the uncertainties (also asserted earlier). The robust optima (b, e), on the other hand, have lower variances in the QoIs except for a couple of realizations where the drag is significantly larger then all the other samples. Overall, the optimal design under the presence of environmental uncertainty is considerably more resilient to the input randomness as compared to its deterministic counterpart. Upon adding the operational uncertainties (c, f), as expected and discussed earlier, the robustness of the optimal design only decreases marginally due to increased variations in the QoIs.

The box-plot for the drag coefficient (in terms of drag counts) at different optimums for $e^N$ method and DLR $\gamma$ model are presented in Fig 10. The deterministic optimum for both the approaches shows a large and nearly the same average drag. The variability is however, higher for DLR $\gamma$ model, which can be attributed to a large number of realizations with significantly early transition and stronger shock waves as shown in Fig 8 (a, d). The robust optimums (environmental uncertainties) for both approaches shows roughly a 45% reduction in drag and a considerably lower variability. The almost-deterministic drag count for DLR $\gamma$ model can be attributed to a relatively low scattering of transition locations as shown in Fig 8 (e). Upon adding the operational uncertainties, the mean and the variance of the drag count increases slightly for both the approaches.

The overall accuracy of the optimization is driven by many factors, of which, in the present study, the accuracy of transition prediction was the most important. The estimation of transition location using the recently developed intermittency-based model was found to be very close (within 2%) to that obtained using the traditional linear stability theory method. Moreover, optimal airfoil shapes (deterministic and robust) obtained using DLR $\gamma$ model were found to be close to those obtained with $e^N$ method. The overall cost of the optimization process is directly influenced by the total number of black-box evaluations. A single evaluation on 128 processors take around 45 and 25 minutes for $e^N$ method and DLR $\gamma$ model, respectively. This computational cost is marginal for the DoE phase as it can be parallelized. However, the difference quickly grows as we increase the number of sequential infill samples. Therefore, the DLR $\gamma$ model with its inbuilt (on-the-fly) transition prediction capability outperforms the $e^N$ method which relies on a periodic

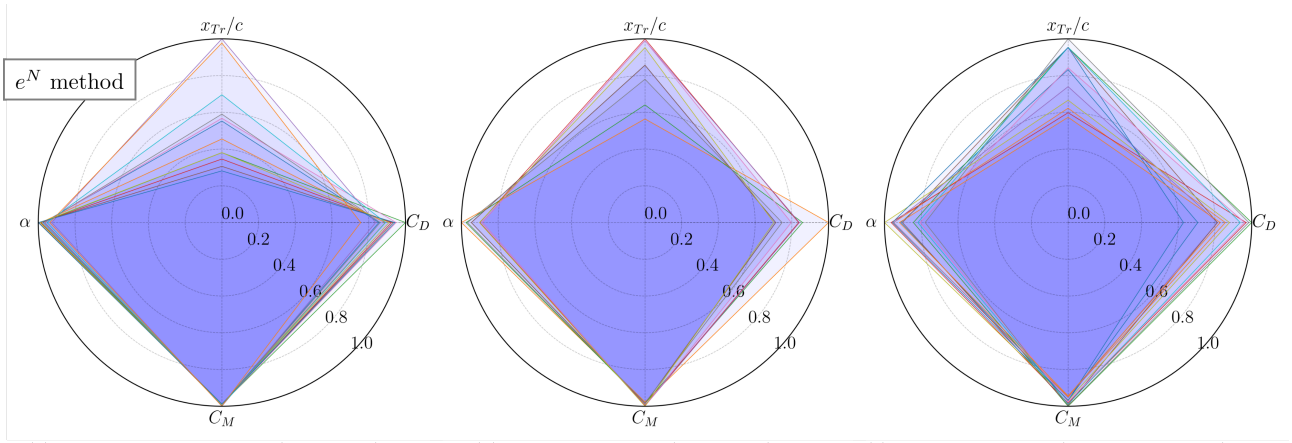


(a) Deterministic Optimum $(N_{TS}, N_{CF})$, $C_D$ (b) Robust Optimum $(N_{TS}, N_{CF})$, $\mu_{C_D}$ (c) Robust Optimum $(N_{TS}, N_{CF}, M, C_L)$, $\mu_{C_D}$

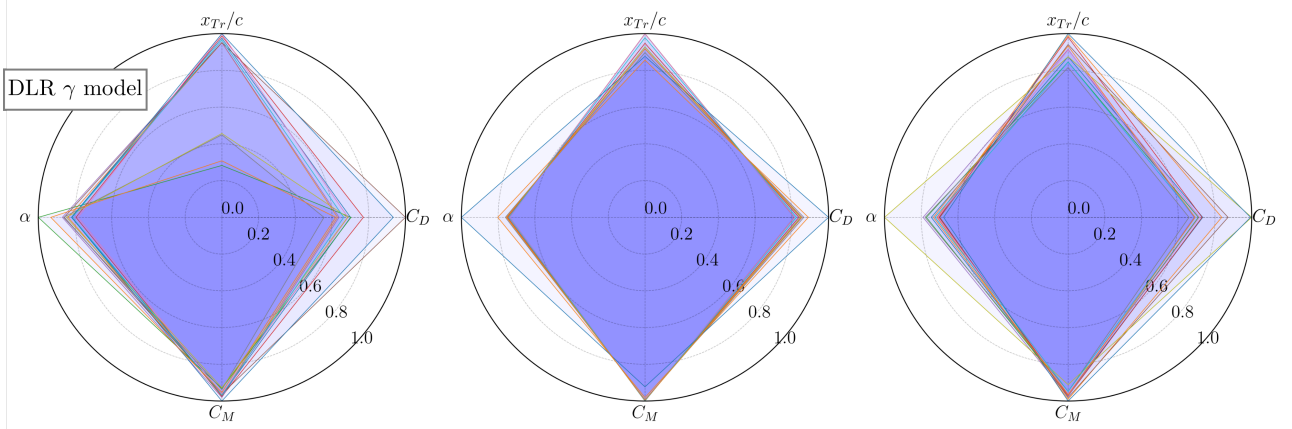


(d) Deterministic Optimum $(T_u)$, $C_D$ (e) Robust Optimum $(T_u)$, $\mu_{C_D}$ (f) Robust Optimum $(T_u, M, C_L)$, $\mu_{C_D}$

FIG 9. Polar graphs of four aerodynamic QoIs - angle of attack $\alpha$, moment coefficient $C_M$, drag coefficient $C_M$ and transition location w.r.t. chord length $x_{Tr}/c$, at different optimums for $e^N$ method and DLR $\gamma$ model. The polygons (colored) represent the realizations of the normalized QoIs. Subfigures (a, b, c) and (d, e, f) correspond to $e^N$ method and DLR $\gamma$ model, respectively.

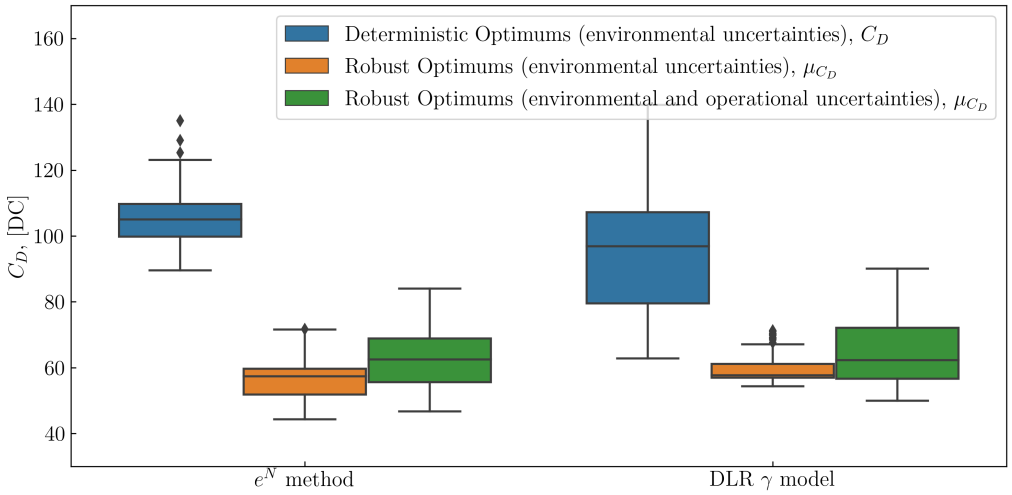


FIG 10. Box plot of optimal configurations under environmental and operational uncertainties.

convergence in $x_{Tr}$. Additionally, a reasonably low number of the parameters settings is required for the stability-based transition transport model. The above-mentioned, therefore, makes the DLR $\gamma$ model a suitable choice to carry out an already expensive robust optimization study.

## 5. CONCLUSIONS

The potential fuel efficiency gains promised by laminar configurations might not be realized in real-world situations using commonly applied inverse design methodologies. A robust design configuration of laminar airfoils (wings) must be sought to maintain a high fuel efficiency under the presence of environmental and operational uncertainties. Direct optimization allows to derive realistic configurations that are able to extend the laminarity until (or close to) the shock location thereby delaying the transition and minimizing the drag. Since the configurations obtained have been optimized only at the nominal values, under the presence of uncertainties in environmental and operational conditions, these design become unstable and can quickly result in fully turbulent flow. This problem can be resolved by quantifying and propagating the uncertainties towards the QoIs and using their statistic(s) to perform optimization enabling new configurations that are robust against the changes in environmental and operational conditions.

A robust optimization framework has been used for extending the natural laminar flow region of an infinite swept wing. An initial study using only the deterministic optimization showed that the optimum is not resilient against the uncertainties in environmental conditions for both the transition prediction approaches ($e^N$ method and DLR $\gamma$ model). Once the uncertainties were incorporated in the optimization process (using a surrogate-based uncertainty quantification approach), the average performance was significantly improved resulting in overall robust configurations. These robust designs promote - (i) delayed transitions (extended laminarity), (ii) weaker shock waves, (iii) realistic pressure profiles, and (iv) stability. Moreover, the robust optimums favor a smooth variation in transition location w.r.t. the instabilities, unlike the deterministic optimums that feature sudden transitions triggering fully turbulent flow. To perform an efficient robust optimization study, the recently developed DLR $\gamma$ transition transport model was found to be more economical and easy-to-use as compared to the traditional $e^N$ method.

In the future, larger design space (exploration mode) can be investigated to seek robust design with larger extent of laminarity. The thickness based constraint can be replaced with a wing-box constraint to obtain further realistic configurations. Also, other sources of uncertainties can be considered e.g. randomness in Reynolds number, model form uncertainties etc. Lastly, a crossflow extension of the DLR $\gamma$ model can be used to account for crossflow instabilities which is vital for investigating more complex configurations.

Contact address:

jigar.parekh@dlr.de

## References

[1] Publications Office of the European Union. Flightpath 2050 : Europe's vision for aviation : maintaining global leadership and serving society's needs. 6 2011. DOI: 10.2777/50266.

[2] North Atlantic Treaty Organization. Advisory Group for Aerospace Research, Development. Fluid Dynamics Panel, and Von Karman Institute for Fluid Dynamics. Aircraft Drag Prediction and Reduction. AGARD report. North Atlantic Treaty Organization, Advisory Group for Aerospace Research and Development, 1985.

[3] G. Redeker, K. H. Horstmann, H. Köster, P. (1) Thiede, and J. (1) Szodruch. Design of a Natural Flow Glove for a Transport Aircraft. In AIAA CP 907, pages 375–384. AIAA, 1990. LIDO-Berichtsjahr=1990, pages=10,.

[4] Doug McLean. Understanding Aerodynamics. pages 380–382, 2013.

[5] G. Schrauf. Evaluation of the A320 hybrid laminar fin experiment. 2000.

[6] Richard L. Campbell and Michelle N. Lynde. Natural Laminar Flow Design for Wings with Moderate Sweep. DOI: 10.2514/6.2016-4326.

[7] Michelle N. Lynde, Richard L. Campbell, Melissa B. Rivers, Sally A. Viken, David T. Chan, A. Neal Watkins, and Scott L. Goodliff. Preliminary results from an experimental assessment of a natural laminar flow design method. AIAA Scitech 2019 Forum, 2019. DOI: 10.2514/6.2019-2298.

[8] T. Streit, S. Wedler, and M. Kruse. DLR natural and hybrid transonic laminar wing design incorporating new methodologies. Aeronautical Journal, 119:1303–1326, 11 2015. DOI: 10.1017/S0001924000011283.

[9] S. N. Skinner and H. Zare-Behtash. State-of-the-art in aerodynamic shape optimisation methods. Applied Soft Computing, 62:933–962, 1 2018. DOI: 10.1016/J.ASOC.2017.09.030.

[10] Zhong Hua Han, Jing Chen, Ke Shi Zhang, Zhen Ming Xu, Zhen Zhu, and Wen Ping Song. Aerodynamic shape optimization of natural-laminar-flow wing using surrogate-based approach. AIAA Journal, 56:2579–2593, 6 2018. DOI: 10.2514/1.J056661.

[11] Zhao Huan, Gao Zheng-Hong, Wang Chao, and Gao Yuan. Robust design of high speed natural-laminar-flow airfoil for high lift. AIAA SciTech Forum - 55th AIAA Aerospace Sciences Meeting, 2017. DOI: 10.2514/6.2017-1414.

[12] Ronald D Joslin. AIRCRAFT LAMINAR FLOW CONTROL 1. Annu. Rev. Fluid Mech, 30:1–29, 1998.

[13] Jed Hollom and Ning Qiny. Robustness of natural laminar flow airfoil drag optimization to transition amplification factor. 18th AIAA/ISSMO Multidisciplinary Analysis and Optimization Conference, 2017, 2017. DOI: 10.2514/6.2017-3144.

[14] Christian Sabater, Philipp Bekemeyer, and Stefan Görtz. Robust Design of Transonic Natural Laminar Flow Wings Under Environmental and Operational Uncertainties. AIAA Journal, 60:767–782, 2 2022. DOI: 10.2514/1.J060676.

[15] Christian Sabater, Philipp Bekemeyer, and Stefan Görtz. Efficient bilevel surrogate approach for optimization under uncertainty of shock control bumps. AIAA Journal, 58:5228–5242, 2020. DOI: 10.2514/1.J059480.

[16] Alexander I.J. Forrester and Andy J. Keane. Recent advances in surrogate-based optimization. Progress in Aerospace Sciences, 45(1):50–79, 2009. DOI: https://doi.org/10.1016/j.paerosci.2008.11.001.

[17] Philipp Bekemeyer, Anna Bertram, Derrick Armando Hines Chaves, Mateus Dias Ribeiro, Andrea Garbo, Anna Kiener, Christian Sabater Campomanes, Mario Stradtner, Simon Wassing, Markus Widhalm, Stefan Görtz, Florian Jäckel, Robert Hoppe, and Nils Hoffmann. Data-Driven Aerodynamic Modeling Using the DLR SMARTy Toolbox. American Institute of Aeronautics and Astronautics Inc, AIAA, 2022. DOI: 10.2514/6.2022-3899.

[18] I.M Sobol'. On the distribution of points in a cube and the approximate evaluation of integrals. USSR Computational Mathematics and Mathematical Physics, 7(4):86–112, 1967. DOI: https://doi.org/10.1016/0041-5553(67)90144-9.

[19] Zhong-Hua Han, Stefan Görtz, and Ralf Zimmermann. Improving variable-fidelity surrogate modeling via gradient-enhanced kriging and a generalized hybrid bridge function. Aerospace Science and Technology, 25(1):177–189, 2013. DOI: https://doi.org/10.1016/j.ast.2012.01.006.

[20] Donald R. Jones, Matthias Schonlau, and William J. Welch. Efficient Global Optimization of Expensive Black-Box Functions. Journal of Global Optimization, 13:455–492, 1998. DOI: 10.1023/A:1008306431147/METRICS.

[21] G. Schrauf. Status and perspectives of laminar flow. The Aeronautical Journal, 109:639–644, 2005. DOI: 10.1017/S000192400000097X.

[22] Géza Schrauf. Large-Scale Laminar Flow Tests Evaluated with Linear Stability Theory. https://doi.org/10.2514/1.9280, 41:224–230, 5 2012. DOI: 10.2514/1.9280.

[23] Brenda M. Kulfan. Universal Parametric Geometry Representation Method. https://doi.org/10.2514/1.29958, 45:142–158, 5 2012. DOI: 10.2514/1.29958.

[24] Thomas Gerhold. Overview of the Hybrid RANS Code TAU. MEGAFLOW - Numerical Flow Simulation for Aircraft Design, pages 81–92, 10 2005. DOI: 10.1007/3-540-32382-1_5.

[25] J. Drofelnik and A. D. Ronch. 2.5D+ TAU User Guide. DLR, German Aerospace Center TR, 2017.

[26] J. V. Ingen. A suggested semi-empirical method for the calculation of the boundary layer transition region. 1956.

[27] Daniela Gisele François, Andreas Krumbein, Normann Krimmelbein, and Cornelia Grabe. Simplified stability-based transition transport modeling for unstructured computational fluid dynamics. Journal of Aircraft, pages 1–12, 2023.

[28] A. Krumbein, N. Krimmelbein, and G. Schrauf. Automatic transition prediction in hybrid flow solver, part 1: Methodology and sensitivities. Journal of Aircraft, 46(4):1176–1190, 2009. DOI: 10.2514/1.39736.

[29] Géza Schrauf. COCO—A Program to Compute Velocity and Temperature Profiles for Local and Nonlocal Stability Analysis of Compressible, Conical Boundary Layers with Suction. ZARM TR, 1998.

[30] Géza Schrauf. LILO 2.1–User's Guide and Tutorial. GSSC TR 6, Bremen, Germany, Sept. 2004, modified for Ver. 2.1, 2006.

[31] R. B. Langtry and F. R. Menter. Correlation-based transition modeling for unstructured parallelized computational fluid dynamics codes. AIAA journal, 47(12):2894–2906, 2009.

[32] Daniela G François, Andreas Krumbein, and Normann Krimmelbein. Crossflow Extension of a Simplified Transition Transport Modelfor Three-Dimensional Aerodynamic Configurations. In AIAA AVIATION Forum, 2022.

[33] S. Helm, D. G. François, C. Grabe, J. Parekh, and P. Bekemeyer. CFD-basierte Transitionsvorhersage für den Entwurf von Laminarflugzeugen (abstract accepted). In DLRK, 2023.

[34] Géza Schrauf. Industrial view on transition prediction. Recent Results in Laminar-Turbulent Transition, pages 111–122, 2004. DOI: 10.1007/978-3-540-45060-3_9.

[35] Martin Kruse, Albert Küpper, Rouven Petzold, and Federico Munoz. Determination of the critical cross flow N-factor for the low-speed wind tunnel braunschweig (DNW-NWB). Notes on Numerical Fluid Mechanics and Multidisciplinary Design, 136:251–261, 2018. DOI: 10.1007/978-3-319-64519-3_23.

[36] Mack and L. M. Transition prediction and linear stability theory. ltt, 1977.

[37] R Radespiel and W Heinze. SFB 880: Fundamentals of high lift for future commercial aircraft. CEAS Aeronautical Journal, 2014. DOI: 10.1007/s13272-014-0103-6.

[38] Jean Perraud, Hugues Deniau, and Grégoire Casalis. Overview of transition prediction tools in the elsa software. In ECCOMAS 2014, 2014.